8

Wavelets in atomic physics and in solid state physics

J.-P. ANTOINE

Institut de Physique Théorique,
Université Catholique de Louvain, Belgium

Ph. ANTOINE and B. PIRAUX

Laboratoire de Physique Atomique et Moléculaire,
Université Catholique de Louvain, Belgium

Abstract

In the field of atomic and solid state physics, wavelet analysis has been applied so far in three different directions: (i) time–frequency analysis of harmonic generation in laser–atom interactions; (ii) *ab initio* electronic structure calculations in atoms and molecules; and (iii) construction of localized bases for the lowest Landau level of a 2-D electron gas submitted to a strong magnetic field. We survey these three types of applications, with more emphasis on methods than on precise results.

8.1 Introduction

There are two ways in which wavelets could play a role in atomic physics and possibly in solid state physics.

First one may envisage them as *physical objects*, namely quantum states or wave functions. It is commonplace to remark that coherent states (CS) have a privileged role in atomic physics. Laser–atom interactions, revival phenomena, Rydberg wave packets and various semi-classical situations are all instances in which a coherent state description is clearly well-adapted. Of course, what is implied here are *canonical* CS, associated to the harmonic oscillator or the electromagnetic field [36]. But wavelets are also coherent states, namely those associated to the affine groups in various space dimensions, as we have seen in Chapter 2 (see [1] for a review on coherent states). Thus wavelets could well be thought of as convenient substitutes for canonical CS. However, this suggestion is still speculative at the present moment, very little has been achieved in this direction.

Actually there have been so far only a few applications of wavelets in atomic physics and in solid state physics, and in all cases they were used as a *mathematical tool*. We will survey these applications in the present chapter, with more emphasis on methods than on actual results. More precisely, we will describe three main directions of research.

(1) When an atom is hit by a very intense, ultra-short laser pulse, it may emit light, in the form of harmonics of the incident electromagnetic field. The time profile of the emission spectrum reveals new information on the dynamics of this interaction process. Clearly, this time profile is out of reach of the traditional Fourier spectral methods, a time–frequency analysis is required. This phenomenon has received recently much attention, both experimentally and theoretically, although the numerical simulations are mostly limited to one-electron atoms. Notice that both the Continuous Wavelet Transform (CWT) and the Windowed Fourier Transform (just another name for canonical CS!) have been used.
(2) Both the extension of these phenomena to multi-electron atoms and the self-consistent electronic structure calculations (Hartree–Fock and generalizations) require the use of appropriate orthogonal bases for the description of the radial part of wave functions. Here (discrete) wavelet bases (or even frames) could adequately replace traditional plane waves or atomic orbital (LCAO) bases. The reason is that orthogonal wavelet bases with good localization properties will minimize the number of terms required for an accurate calculation of wave functions and related observable quantities. This program has been fulfilled in *ab initio* electronic structure calculations, in atoms, molecules and crystals. The crucial feature is the narrow support of the wavelets constituting an orthonormal basis. This is in fact the most active line of research with wavelets in solid state physics.
(3) Another application in solid state physics deals with a two-dimensional physical system, namely an electron gas submitted to a strong magnetic field, the set-up of the quantum Hall effect. Here wavelets yield various bases for the lowest Landau level, a necessary step for the description of the fractional quantum Hall effect.

Except for some marginal cases, these three topics are the most significant applications of wavelets in atomic and solid state physics. In our opinion, they are sufficiently promising to establish the credentials of wavelet methods in those fields of physics. Both the CWT, as a precise time-frequency analysis tool, and discrete (bi)orthogonal wavelet bases offer great potential for novel physical applications.

8.2 Harmonic generation in atom–laser interactions

8.2.1 The physical process

When an atom is exposed to a strong laser pulse, two competing processes may occur, the ionization of the atom and the emission of light. This emission process results from the oscillations of the atomic dipole at frequencies which are odd multiples (odd harmonics) of the driving field frequency (even harmonics are forbidden by parity conservation). Harmonic generation provides an efficient source of coherent soft X-rays [44], which explains the potential interest of the phenomenon for applications. Now for a full understanding of the emission mechanism, one would like to answer questions like: When are harmonics emitted during the optical cycle? What is the time evolution of the emission during the laser pulse? . . . . Clearly, this is beyond standard spectral methods, a time–frequency analysis is needed here.

Let us consider for simplicity the case of atomic hydrogen exposed to a strong laser pulse whose electric field is described classically as: $\mathbf{E} = \mathbf{E}_0(t) \cos \omega t$, where $\mathbf{E}_0$ is the pulse envelope. The atomic response to such a pulse is highly nonlinear, which leads to various unexpected phenomena. One of them is the emission by the atom of high order harmonics of the driving field. According to the semiclassical interpretation [18, 39], this harmonic generation results from the following two-step mechanism. The electron tunnels through the potential barrier formed by the combined Coulomb and electromagnetic (e.m.) fields. When it is outside, it is accelerated by the laser e.m. field and may be driven back to the residual ion. There, it may either be scattered, or recombine back into the ground state, emitting a harmonic photon. This interpretation is supported by quantum-mechanical models [41], in which the time-dependent dipole moment is expressed as the sum of the contributions from the electron trajectories in the continuum.

The resulting emission spectrum exhibits characteristic features which depend on the laser intensity. At low laser intensity, the spectrum of the emitted radiation decreases rapidly for increasing harmonic order, as expected. At high laser intensity, the spectrum changes drastically: after a rapid decrease for the first orders, it exhibits a long plateau, followed by a sharp cut-off. A spectacular example is given in Figure 8.1. Experimentally, harmonic orders as high as the 135th order have been observed with a Nd-Glass laser, which corresponds to a wavelength of 7.8 nm, i.e. in the soft X-ray (XUV) regime [43, 46]. The nonlinear character of the atomic response is manifested, for instance, by the fact that, in the spectrum of Figure 8.1, all the harmonics from the 69th to the 109th have almost equal intensity (hence the word 'plateau'), whereas the following ones drop dramatically.

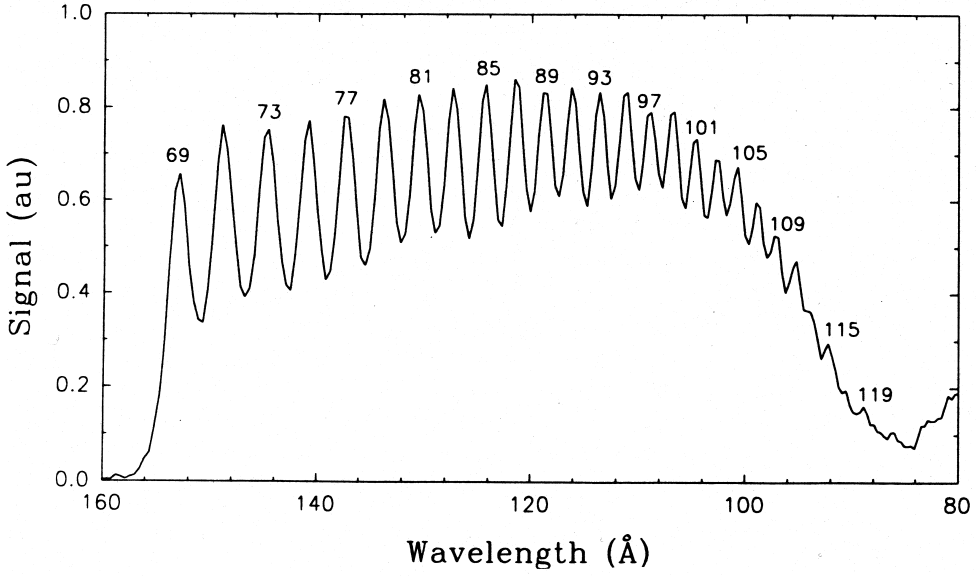

Fig. 8.1. Harmonic spectrum obtained in He for $\lambda = 1053$ nm and a laser intensity of 3×10^{14} Wcm^{-2}; in this case, the first harmonics up to about the order 67 are filtered out. Note the sharp cut-off around the order 113 (from [51]).

In the low intensity regime, the atomic response may be calculated by perturbation theory. But in the intense field regime, where the external field is of the same order or higher than the binding atomic field, nonperturbative methods are needed. A possible approach consists in solving (numerically) the time-dependent Schrödinger equation [38]. Atomic dipoles calculated by this method may be analysed with the standard Fourier spectral method, and the corresponding harmonic spectra exhibit the global features described above. However, a time–frequency analysis provides a deeper understanding of the mechanism: it allows to determine the time profile of each individual harmonic and from this one may deduce that harmonic emission takes place only when the electron is close to the nucleus.

8.2.2 Calculation of the atomic dipole for a one-electron atom

As mentioned above, the primary cause of harmonic emission is that the electron of the atomic hydrogen oscillates back and forth under the influence of the laser field, hence creates a dipole moment $d(t)$. Then, according to the Larmor formula, the energy radiated between frequencies ω and $\omega + d\omega$ is proportional to $|\widehat{a}(\omega)|^2$, where $\widehat{a}(\omega)$ is the Fourier transform of the dipole acceleration $a(t) = \ddot{d}(t)$. Therefore the problem consists in calculating

(numerically) the acceleration $a(t)$ from the time-dependent Schrödinger equation:

$$i\frac{\partial}{\partial t}\psi(\mathbf{r}, t) = (H_{at} + \mathbf{A}(t)\cdot\mathbf{p})\,\psi(\mathbf{r}, t). \tag{8.1}$$

Here, H_{at} is the atomic Hamiltonian, $\mathbf{p}$ is the electron momentum, the vector potential $\mathbf{A}$ is written in the dipole approximation, i.e. $\mathbf{A}(\mathbf{r}, t) = \mathbf{A}(t)$ depends on time only, and is treated as a classical variable, and finally the quadratic term $\mathbf{A}^2$ has been gauged away. It is convenient to take the vector potential along the z-axis:

$$\mathbf{A}(t) = A_o(t)\,\sin\omega_L t\,\hat{\mathbf{e}}_z,$$

where $A_o(t)$ is the envelope of the pulse and ω_L the laser frequency. Notice that the shape of the pulse influences considerably the harmonic emission. In terms of the solution $\psi(\mathbf{r}, t)$ of the Schrödinger equation (8.1), the atomic dipole along the z-axis reads

$$d(t) = \langle\psi(\mathbf{r}, t) \mid z \mid \psi(\mathbf{r}, t)\rangle. \tag{8.2}$$

Using Ehrenfest's theorem, the corresponding acceleration may be written as:

$$a(t) = \ddot{d}(t) = -\langle\psi(\mathbf{r}, t) \mid \frac{z}{r^3} \mid \psi(\mathbf{r}, t)\rangle + \frac{\partial A_z}{\partial t}. \tag{8.3}$$

The next step is to expand $\psi(\mathbf{r}, t)$ in an appropriate basis. For obvious reasons, one takes spherical harmonics for the angular part. As for the radial part, a convenient choice is a Coulomb Sturmian basis $\{S_{nl}(r)\}$, because of its good convergence properties [50]. Notice that complex Sturmian functions are required, in order to reproduce the correct asymptotic behaviour (outgoing wave) of the wave function [34]. Thus we write:

$$\psi(\mathbf{r}, t) = \sum_{nlm} a_{nl}(t)\,\frac{S_{nl}(r)}{r}\,Y_l^m(\theta, \varphi). \tag{8.4}$$

Inserting the expansion (8.4) into the Schrödinger equation (8.1), one obtains a set of first order differential equations for the coefficients $a_{nl}(t)$, that can be readily solved numerically (but without approximation), to yield the dipole acceleration $a(t)$. A typical result is shown in Figure 8.2. The dipole acceleration presents a region of rapid oscillation, starting well before the maximum of the pulse (taken as the origin of time) is reached. This region corresponds to the generation of harmonics, as will be confirmed by the time–frequency analysis.

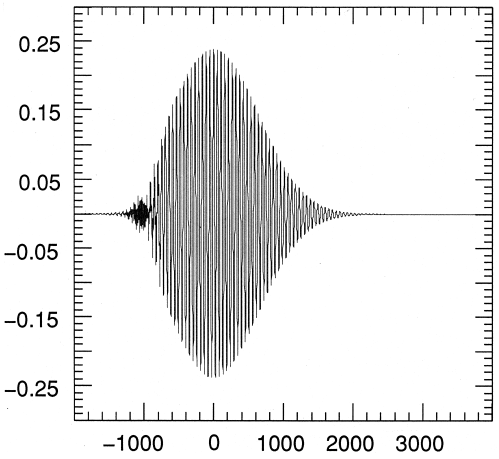

Fig. 8.2. Acceleration of the atomic dipole as a function of time (both in atomic units). This dipole is the result of the interaction of atomic hydrogen with a strong laser pulse of frequency $\omega_L = 0.118$ atomic units. The pulse envelope $A_o(t)$ is Gaussian and its full width at half maximum is 20 optical cycles. The peak intensity is 2×10^{15} Wcm^{-2}.

8.2.3 Time–frequency analysis of the dipole acceleration: H(1s)

Taking now the Fourier transform $\widehat{a}(\omega)$ of the dipole acceleration $a(t)$, one obtains the power spectrum. Figure 8.3 shows two typical spectra. The left one corresponds to a rather low frequency e.m. field ($\omega_L = 0.047$ a.u.) and moderate intensity. The spectrum exhibits a large number of odd harmonics of the laser frequency, which form a long 'plateau', with a sharp cutoff beyond $\omega = 33\omega_L$. On the right, we show the spectrum corresponding to the high intensity pulse of Figure 8.2. Of course, no time localization is provided. When is each harmonic emitted? What is its time profile? Answering those questions requires a time–frequency analysis of the acceleration, as discussed in Chapter 1, section 1.1:

$$a(t) \mapsto \tilde{a}(\alpha, \tau) = \int_{-\infty}^{\infty} \overline{g_{\alpha\tau}(t)}\, a(t)\, dt. \tag{8.5}$$

In this expression $\alpha > 0$ is the scale parameter and τ the time parameter (usually denoted a and b, respectively, as in Chapter 1). Two types of time–frequency analysis have been used in the present problem, namely

- a Gabor transform, corresponding to $g_{\alpha\tau}(t) = e^{it/\alpha}\, e^{-\frac{1}{2}(t-\tau)^2}$ ($g_{\alpha\tau}(t)$ is then a canonical coherent state)
- a wavelet transform, with a (truncated) Morlet wavelet $g(t) = e^{i\omega_o t} e^{-t^2/2}$ and $g_{\alpha\tau}(t) = \alpha^{-1/2} g(\alpha^{-1}(t-\tau))$.

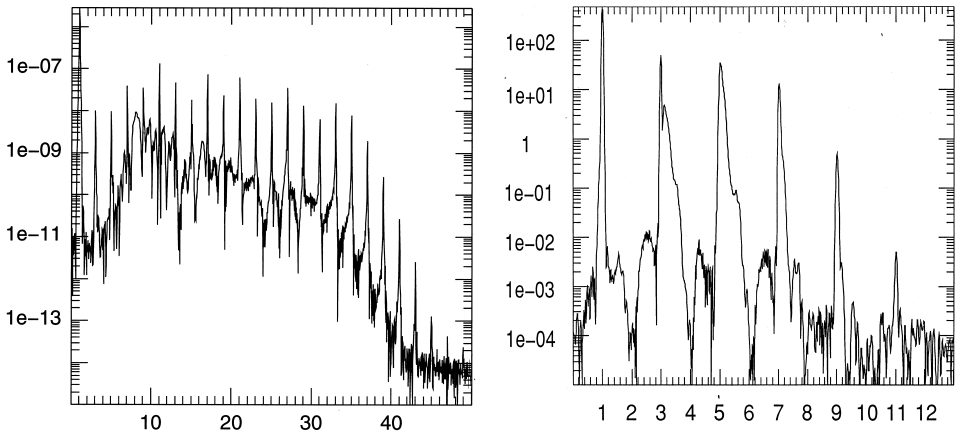

Fig. 8.3. (Left) Power spectrum (arbitrary units) as a function of harmonic order, in the case of the interaction of atomic hydrogen with a laser pulse of frequency $\omega_L = 0.047$ a.u. and (low) peak intensity 10^{14} Wcm^{-2}. The pulse has a 4 optical cycle sine-square turn-on and -off and a flat top of 16 optical cycles. (Right) Harmonic spectrum of the high intensity pulse of Fig. 8.2.

The information contained in the function $\tilde{a}(\alpha, \tau)$ may be exploited according to several different strategies. First, one may calculate the emission strength as a function of time, for a given frequency, that is, one evaluates $\tilde{a}(\alpha, \tau)$ for fixed α. One can also estimate the instantaneous frequency of emission of a given harmonic, as a function of time (τ). Alternatively, one may determine the full harmonic spectrum for a fixed time $\tau = t_o$, that is, consider $\tilde{a}(\alpha, t_o)$ as a function of α.

This technique has been applied successfully in the case of a hydrogen atom, both in its ground state and in the metastable state 2s, or a simplified model thereof (two-level atom), and considerable insight has been gained in the physical mechanism of harmonic generation. Let us give some details on the various aspects of the analysis.

8.2.3.1 Time dependence of harmonic emission in H(1s)

Let us begin with a hydrogen atom in its ground state. According to the semiclassical description, the so-called two-step model [18, 39], harmonic emission takes place only when the electron is close to the nucleus (see Section 8.2.1). Using a time–frequency analysis at fixed frequency, with a window whose bandwidth is smaller than $2\omega_L$, one is able to estimate the time profile of individual harmonics in the emitted radiation, as indicated by the following results.

(i) Time profile of harmonics: Choosing for α in (8.5) the inverse of a fixed odd multiple of the laser frequency, one obtains the time profile of the corresponding harmonic [3]. First, a Gabor analysis yields the global shape of each harmonic (Figure 8.4, left). Two interesting points are visible on this picture. First, the emission of each harmonic starts at a given characteristic time, which depends on the laser intensity. Then, as their order increases, the harmonics are emitted during shorter time intervals. This implies that the linewidth of higher harmonics should broaden with their order. The fact that harmonic emission stops before the field has reached its maximum amplitude (in $t = 0$) is due to the rapid excitation and ionization of the atom. This effect has been observed experimentally [52].

The picture may be refined by using a wavelet analysis (using a Morlet wavelet). Figure 8.4 (right) shows the time profile of the 9th harmonic of the same pulse. A fine structure appears, which is $2\omega_L$-periodic, in agreement with the semiclassical interpretation. Notice that, since the time resolution is better than half the optical period, the filter bandwidth is larger than $2\omega_L$. Therefore several harmonics are accepted simultaneously by the filter.

The same technique reveals also how the time profile depends on the position of the harmonic in the spectrum. Take for instance the case depicted in Figure 8.3 (left), which corresponds to a low frequency regime

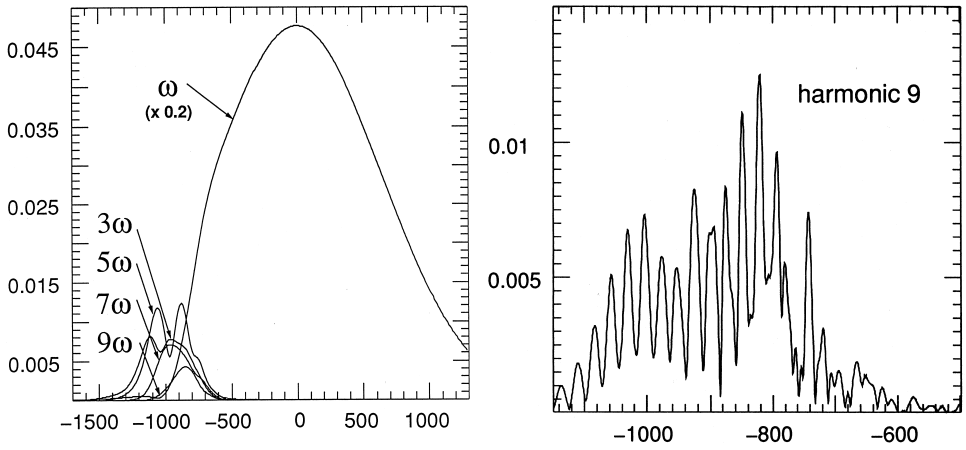

Fig. 8.4. (Left) Time profile (from Gabor analysis) of the odd harmonics (1 – 9) produced as a result of the interaction of atomic hydrogen with the same laser pulse as in Fig. 8.2 (time is in atomic units). (Right) Time profile (from wavelet analysis) of the 9th harmonic emitted in the same pulse. Note that the frequency bandwidth of the pulse exceeds in this case $2\omega_L$.

($\omega_L = 0.047$ a.u.). The wavelet analysis shows that the time profile of harmonic 21, in the plateau (a), and that of harmonic 39, in the cutoff (b), are totally different (see Figure 8.5) [6]. The emission process is clearly more complex in the first case. In the case of a harmonic beyond the cutoff, one sees only one peak per half optical cycle. On the contrary, the time profile of harmonic 21 has two peaks for each half optical cycle. This behaviour is in agreement with the quantum-mechanical model of Lewenstein *et al.* [41], at least in the limit of high field and low frequency (the high frequency case is also interesting, but physically more complex). In the cutoff, there is only one electron trajectory contributing to the emission [42]. As a result, the decrease in the spectrum beyond the cutoff is very smooth and regular. By contrast, in the plateau where several electron trajectories lead to the same harmonic, the resulting interference leads to a highly structured spectrum as function of the harmonic order [42]. For instance, the presence of two peaks per half optical cycle in harmonic 21 reflects the existence of two return times contributing to the emission of the same harmonic, that is, two interfering electron trajectories. By analysing the harmonic emission in the time domain rather than in the frequency domain, the contributions of the different electron trajectories in the continuum are naturally separated [5]. In addition, the wavelet analysis also reveals a good agreement between the time-dependent Schrödinger equation model and the strong field approximation (SFA) model, for harmonics close to or beyond the cutoff [6].

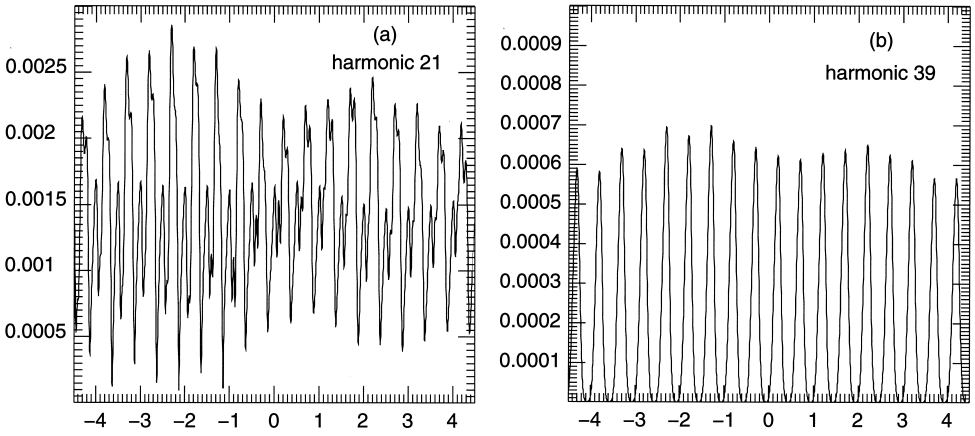

Fig. 8.5. (Left) Time profile (from wavelet analysis) of harmonic 21 (in the plateau) for the same conditions as in Fig. 8.3 (left); time is measured in optical periods. (Right) The same for harmonic 39.

(ii) Temporal control of harmonic emission: In the semiclassical description, the electron emits harmonics when it is close to the nucleus. Therefore, the harmonic emission may be controlled if one uses a laser beam with a time-varying polarization. When the polarization is linear, the electron oscillates back and forth, hence it comes periodically close to the nucleus, and harmonics are emitted. When the polarization is elliptic or circular, the electron stays far away and harmonic generation is suppressed. This polarization effect is demonstrated in Figure 8.6, which shows in parallel: (left) the time evolution of the harmonic 9, and (right) the projection of the full wave function on the bare 1s state of atomic hydrogen [4]. The latter measures the probability of the electron being close to the nucleus. Hence it oscillates when the field is linearly polarized, but remains constant in the circular or elliptic cases. As expected, the two curves are in perfect correspondence: the harmonic is totally suppressed when the polarization of the laser beam is circular and it reaches its maxima precisely when the polarization is linear.

In fact, this effect may be exploited further. It has been demonstrated on the basis of the strong field approximation (SFA), that the time profile of the harmonic emission consists of a regular attosecond pulse train [5] (1 attosecond $= 10^{-18}$s). By using a polarization which is linear during a very short period in place of a fixed polarization, it should be possible to select one of

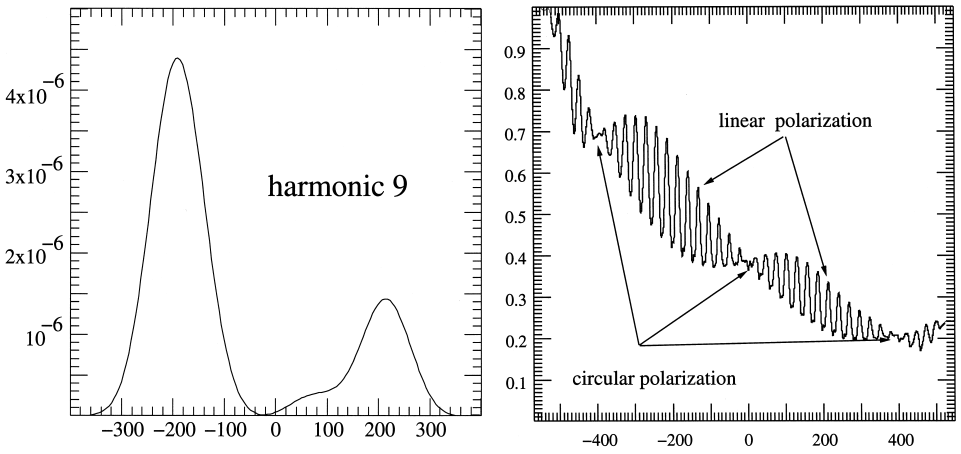

Fig. 8.6. The polarization effect. (Left) Intensity of the 9th harmonic as a function of time (in atomic units) in the case where the atom is exposed to two perpendicularly polarized laser pulses of 10^{14} Wcm^{-2}. The photon energies are 0.118 and 0.110 atomic units, respectively. Both pulses have a flat top and sine-square turn-on and -off. The total duration of the pulse is 20 optical cycles. (Right) Corresponding 1s population, measured by the projection of the full wave function on the bare 1s state of atomic hydrogen (from [4]).

these attosecond pulses of the train. This scheme opens the route to the production of a single intense attosecond pulse.

8.2.3.2 Harmonic emission in H(2s)

The same space localization effect of the harmonic generation takes place if the hydrogen atom is initially in the metastable state 2s [3]. When the latter interacts with a high intensity laser pulse, the system is excited into a linear superposition of many Rydberg states (mainly 8p, 9p and 10p). As a result, ionization is significantly suppressed and hence the atomic dipole does not vanish at the end of the interaction with the pulse. A similar situation occurs in H(1s), at low intensity, but the dynamics is much more complex now, because of the excitation of many atomic states. In order to get an insight into the time evolution of the process, we look again at the time profile of a typical harmonic (the third one), obtained by a Gabor analysis and shown in Figure 8.7(a). The curve shows two pronounced maxima. The left one corresponds to the emission of the harmonic. However the second one (around 1300 a.u.) is due to an atomic frequency which is almost degenerate with $3\grave{o}\omega_L$ and is present during the free evolution of the dipole after the interaction with the pulse. This interpretation is confirmed by an analysis of the population dynamics. We present in Figure 8.7(b) the time evolution of the 1s population (measured again by the projection of the total wave function on the 1s bare atomic state). This population is significant only at two moments: around 1000 a.u. before the maximum of the pulse and then again after

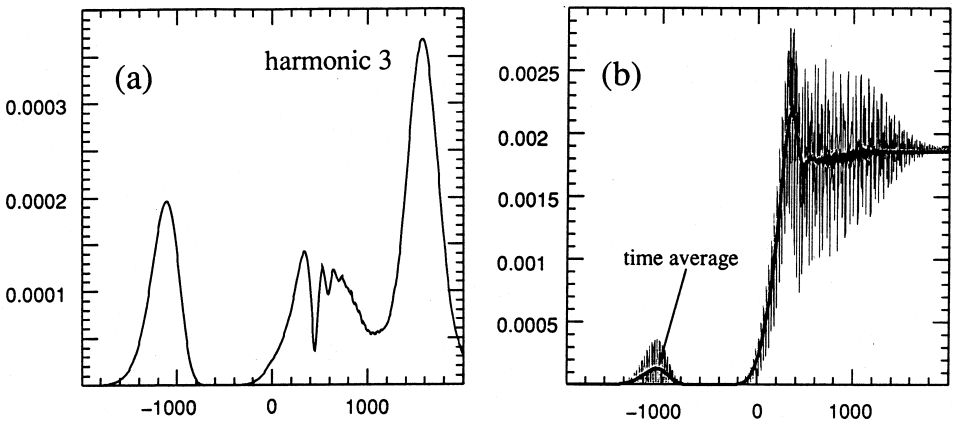

Fig. 8.7. (Left) Time profile (in atomic units) of the third harmonic emitted by atomic hydrogen initially in its 2s state and exposed to a Gaussian pulse of intensity 2×10^{14} Wcm^{-2} and width 20 optical cycles, and laser frequency $\omega_L = 0.118$ a.u. (Right) 1s population as a function of time for the same situation (from [3]).

interaction. In the first region, the 1s population oscillates with frequency $2\omega_L$ around its average, which corresponds to the back and forth oscillation of the electron through the central region of the atom, and the concomitant emission of the harmonic. As for the second region, it manifests a rapid exchange of population between the 1s state and excited states, with no harmonic emission.

8.2.3.3 Instantaneous frequency of emission

Actually, the frequencies of the harmonics are exact odd multiples of the frequency of the driving field only if the laser intensity remains constant. On the contrary, when the laser intensity increases, the frequencies are slightly above the exact multiples of ω_L (blueshift). To visualize that effect, we take a linear ramp as the pulse shape, which produces a long plateau, up to $41\omega_L$. On this spectrum, we perform a Gabor analysis rather than a wavelet one, in order to get a time resolution that is independent of the harmonic order. Then all the harmonics have the same behaviour: the Gabor coefficient grows rapidly in time ($\sim$ intensity) and then reaches a saturation intensity with some oscillations. For a given harmonic, the *instantaneous frequency* of emission is given by the time derivative $\frac{d}{d\tau}\phi(\alpha, \tau)$ of the phase $\phi(\alpha, \tau)$ of the corresponding Gabor coefficient. This notion is familiar in wavelet analysis, since it plays an essential role in the determination of spectral lines [20], but applies in the Gabor case as well. The computation fully confirms the effect: each harmonic is slightly blueshifted up to the moment (indicated by an arrow) when it reaches the saturation plateau (Figure 8.8) [54].

8.2.3.4 Harmonic spectrum at fixed time

Alternatively, one may choose a fixed time $\tau = t_o$ and determine the full harmonic spectrum. The computation has been performed on a two-state model for the atom, both with a Gabor analysis [24], and with a wavelet analysis [21]. The two methods yield very similar results, except that the Gabor spectrum contains more noise, which is due to the presence of the so-called hyper-Raman lines. For the wavelet case, two different wavelets have been used, the standard Morlet wavelet and another one, of compact support, which may have independent interest. This new wavelet is defined as:

$$F(t) = \begin{cases} \frac{1}{2}e^{it}[1 + \cos(t/N)], & t \in [-N\pi, N\pi]. \\ 0, & \text{otherwise} \end{cases} \tag{8.6}$$

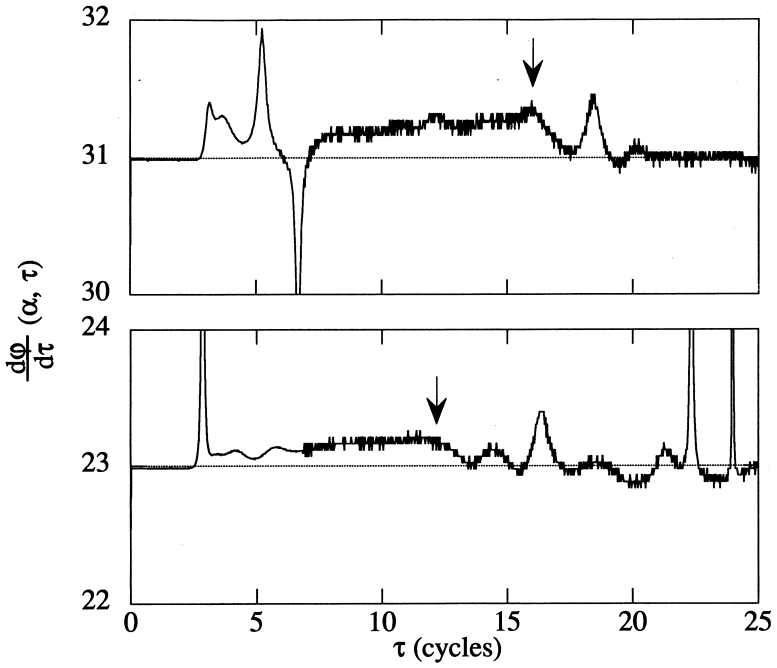

Fig. 8.8. Time derivative of the phase of the Gabor coefficients for $\alpha^{-1} = 23\omega_L$ (lower part) and $31\omega_L$ (upper part). The pulse is a linear ramp of 20 optical cycles and a maximum intensity of 10^{14} Wcm^{-2}. The arrows indicate the times when each harmonic reaches the saturation plateau (from [54]).

Here N is an integer, which gives the number of oscillations of $F(t)$ within its support (it is clear that one needs here a wavelet that oscillates rather fast, a Mexican hat, for instance, would be totally inadequate; typically one takes $N = 30$). Two examples of spectra are shown in Figure 8.9, taken respectively with an F wavelet (a) and a Morlet wavelet (b). As can be seen, there is no significant difference between the two spectra. This confirms that, here as in general, it is not the particular choice of the wavelet that matters, but rather the fact that its shape and the parameters chosen match closely the signal.

8.2.3.5 Which time–frequency method?

It is clear from this discussion that a time–frequency analysis is essential here. Harmonic generation is a highly nonstationary process, whose temporal evolution sheds much light on the actual physical phenomenon. This information is obviously inaccessible to the standard Fourier technique. In addition, as we pointed out already in Chapter 1, Fourier analysis is highly unstable with respect to perturbation, because of its global character. The remedy is to

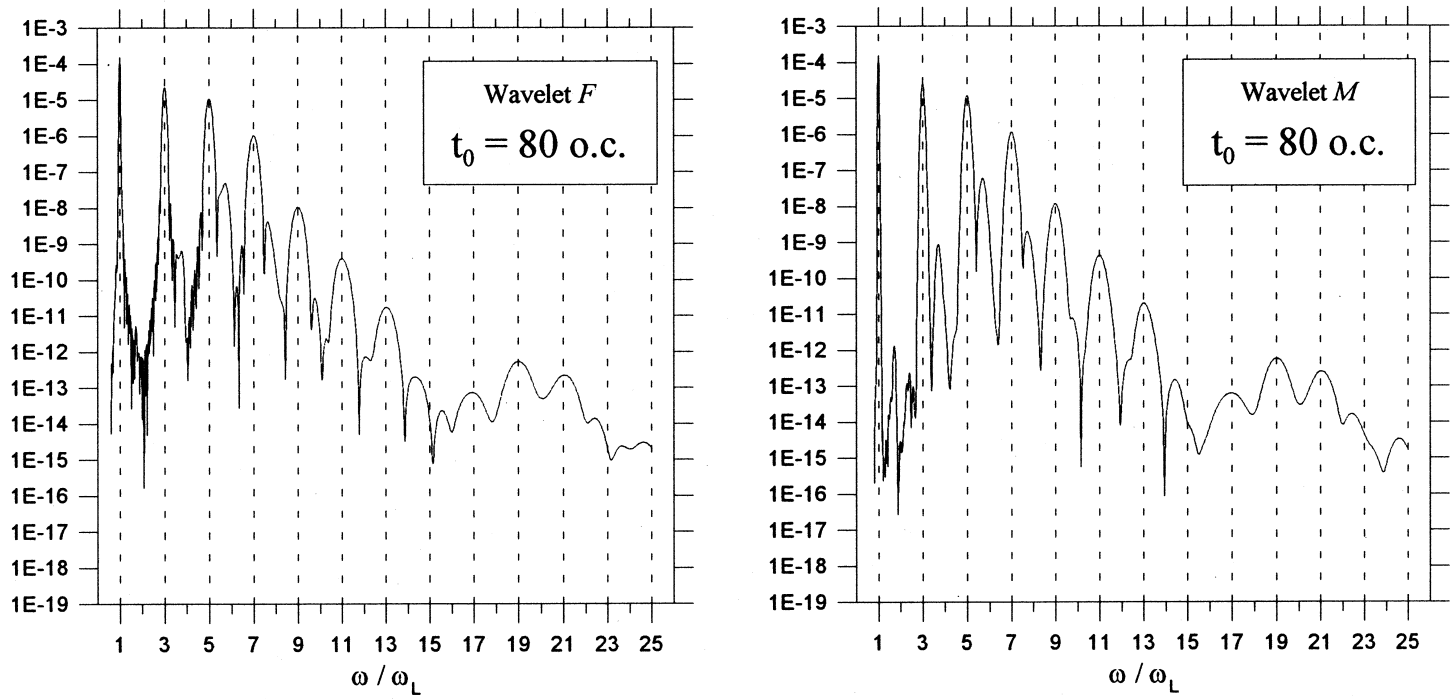

Fig. 8.9. The full harmonic spectrum (wavelet transform of the dipole acceleration) emitted by a two-level atom excited by a laser pulse of intensity 8.8×10^{13} Wcm^{-2}, at time $t_o \equiv \tau = 80$ optical cycles: (a) with the wavelet F of Eq. (8.6); (b) with a Morlet wavelet (private communication from S. De Luca).

represent the signal in terms of localized components, such as Gabor functions or wavelets.

Then a natural question is the choice between wavelets and a Gabor analysis. Globally, the two methods give similar results, provided the time resolution or the bandwidth of the analysing functions are identical. However, wavelet analysis is more appropriate if we want to study *simultaneously* the time profile of several frequencies, keeping the same analysing function. This results of course from the well-known property of wavelets, that $\Delta\omega/\omega$ is constant. As far as harmonic generation is concerned, a wavelet analysis is preferable in the following two cases: (i) for studying very high order harmonics with a time resolution better than the optical cycle, and (ii) when the atomic structure plays a more crucial role; in that case, hyper-Raman lines resulting from atomic transitions may occur in very short time intervals during the interaction with the pulse [3]. On the other hand, it may be inconvenient to make the time resolution depend on the frequency. For example, in order to demonstrate the slight blueshift of the harmonic frequency (Section 8.2.3.3), the time resolution has to be much larger than the optical period since the shift is much smaller than $2\omega_L$, but it should be the same for all harmonics.

So the answer to the question, wavelets or Gabor?, depends essentially on the physics of the problem at hand. The crucial choice is not that of a particular approach, Gabor or wavelets, or even that of a particular analysing function, what really matters is that the parameters of the analysing function be well-adapted to the signal. The case of the fixed time analysis of Section 8.2.3.4 is another confirmation. The conclusion is that *both* methods are needed in fact.

8.2.4 Extension to multi-electron atoms

The analysis of the interaction between a laser pulse and a one-electron atom, discussed in this section so far, rests on the possibility of solving numerically the time-dependent Schrödinger equation. The resulting wave function is then used to estimate various phenomena such as harmonic generation, as discussed above, but also multiphoton ionization, excitation of Rydberg wave packets, etc. In all these cases, the physical processes are complex and largely transient, so that a time–frequency analysis is necessary for a detailed description. Both the CWT and the Gabor analysis prove useful in this respect, as they provide otherwise inaccessible information that complements the traditional tools of atomic physics.

All that is even more true and interesting for two electron atoms, such as He or H^-. But now the situation is much more complicated, because of the correlation between the two electrons. It becomes very hard to solve directly the time-dependent Schrödinger equation and calculate a reasonable two-electron wave packet $\Psi(\mathbf{r}_1, \mathbf{r}_2, t)$, although a clever choice of coordinates may considerably alleviate the difficulty. Few results have been obtained so far. A case in point is a recent paper [40], which treats the case of harmonic generation and ionization from a one-dimensional two-electron He atom. Their conclusion is that, at least for a limited range of laser frequency and intensity, the harmonic generation spectrum in essentially the same as in the one-electron case (for higher intensity, double ionization becomes predominant). This result offers hope that the time–frequency method may be useful to a much wider range of physical situations than those analysed so far.

However, the full three-dimensional problem is still intractable. The difficulty is to find an appropriate basis for expanding the two-electron wave function, in such a way that numerical methods converge fast enough. In fact, only the radial part is subject to discussion, since one likes to keep the spherical harmonics for the angular part, so as to take advantage of the Racah algebra. One may think of several candidates for a good radial basis, such as generalized Sturmian functions, multiresolution-based orthogonal or bi-orthogonal wavelet bases, or even various kinds of frames, for instance those derived from Schrödinger coherent states. But in fact this a particular instance of a more general problem, namely the construction of multi-electronic wave functions, that we now discuss.

8.3 Calculation of multi-electronic wave functions

In any atomic process, the cross-section to be computed is proportional to $|\langle f \mid H_{int} \mid i\rangle|^2$, where H_{int} is the interaction Hamiltonian. The initial state $|\, i\,\rangle$ and the final state $|f\,\rangle$ are atomic states, possibly coupled to a continuum electronic state, in the case of an ionization process. As we have seen in Section 8.2, one may apply various approximations to the interaction Hamiltonian, such as the dipole approximation, the classical treatment of the e.m. field, etc. But the hard problem is to compute the initial and final wave functions. Many standard techniques are available for this purpose, such as variational methods, but the key ingredient is the expansion of the wave function into a suitable basis. Here again, the angular part will be described by spherical harmonics, only the radial part must be found. As mentioned above, a possibility is to use an orthogonal wavelet basis on $[0, \infty]$.

Of course, what we have here is a different use of wavelets, namely as convenient bases for expanding solutions of a partial differential equation. This is a familiar situation, for instance in the resolution of nonlinear PDEs [45]. The advantage of wavelets, as compared to usual bases, resides in their good localization properties. Let us go into some detail.

8.3.1 The self-consistent Hartree–Fock method (HF)

One of the best answers to such questions is given by the self-consistent methods, namely the well-known Hartree–Fock method and its descendants. We shall sketch it very briefly here in order to give some feeling for the technique and the possible use of wavelets for improving it. Further details may be found in standard textbooks, e.g. [15].

The basic idea is to obtain the wave function Ψ for an atom with N electrons by a variational computation

$$\delta\langle\Psi \mid H_{at} \mid \Psi\rangle = 0, \tag{8.7}$$

where H_{at} denotes the atomic Hamiltonian. The total antisymmetry of Ψ (Pauli principle) is enforced by taking it as a Slater determinant of one-electron wave functions:

$$\Psi = \frac{1}{N!}\begin{vmatrix} \phi_1(1) & \dots & \phi_1(N) \\ \vdots & & \vdots \\ \phi_N(1) & \dots & \phi_N(N) \end{vmatrix},$$

where $\phi_i(j)$ is a one-electron wave function ('orbital') of the j^{th} electron. It has the form

$$\phi_i(\mathbf{r}, \text{spin}) = \frac{1}{r} P_{nl}(r)\, Y_l^{m_l}(\theta, \varphi)\chi_{m_s}, \tag{8.8}$$

where $Y_l^{m_l}$ is a spherical harmonic (thus allowing the Racah algebra for angular momentum), χ_{m_s} is a spin orbital, $P_{nl}(r)$ is an unknown radial function and $i \equiv (n, l, m_l, m_s)$ is a collective quantum number ($m_s = \pm\frac{1}{2}$; $m_l = -l, \dots l$; $l = 0, 1, \dots n-1$; $n = 1, 2, \dots$). One usually imposes orthonormality conditions

$$\langle\phi_i \mid \phi_j\rangle = \delta_{ij}$$

$$\int_0^\infty P_{nl}(r)\, P_{n'l'}(r)\, dr = \delta_{nn'}\delta_{ll'}$$

and thus we rewrite the variational equation (8.7) with Lagrange multipliers $\{\lambda_{ij}\}$:

$$\delta\left\{\langle\Psi \mid H_{at} \mid \Psi\rangle + \sum_{i<j} \lambda_{ij}\langle\phi_i \mid \phi_j\rangle\right\} = 0. \tag{8.9}$$

Inserting the ansatz (8.8) into (8.9), one obtains the so-called Hartree–Fock (HF) equations that determine the radial functions $\{P_{nl}(r)\}$:

$$\left\{\frac{d^2}{dr^2} - \frac{l(l+1)}{r^2} + \frac{2}{r}[Z - Y(nl; r) - E_{nl}]\right\} P_{nl}(r) - \frac{2}{r} X(nl; r) = \\ = \sum_{n'} \lambda_{nln'l} P_{n'l}(r). \tag{8.10}$$

In this equation, Y is called the *direct* term and represents a local (spherical) potential, whereas the so-called *exchange* term X is nonlocal. These terms have the following form:

$$Y(nl; r) = \sum_{n'l'} \sum_{k} y_{nl,n'l'}\, Y^k(nl, n'l'; r)$$
$$X(nl; r) = \sum_{n'l'} \sum_{k} x_{nl,n'l'}\, Y^k(nl, n'l'; r) P_{n'l'}(r)$$

where $y_{nl,n'l'}$, $x_{nl,n'l'}$ are coefficients obtained from the angular momentum algebra and

$$Y^k(nl, n'l'; r) = \int_0^\infty \frac{r_<^k}{r_>^{k+1}} P_{nl}(r') P_{n'l'}(r')\, dr', \tag{8.11}$$
$$r_< = \min(r, r'),\ r_> = \max(r, r').$$

Because of the exchange term X, (8.10) is a system of coupled, nonlinear equations in the unknown functions P_{nl}.

The usual technique consists in choosing for P_{nl} a simple trial function and solving the HF equation (8.10) by iteration. Typical choices are a Gaussian or a Slater function $r^{n-1}e^{-\alpha r}$. In general, many terms are needed in the expansion, which makes the method cumbersome or forces drastic truncations, thus leading to unrealistic results.

The alternative possibility that we consider here is to take instead for P_{nl} the elements of a suitable orthonormal wavelet basis. The idea is that the good localization properties of such bases may reduce considerably the number of terms needed. So far, however, this program is still purely speculative, even for two-electron systems. Yet essentially the same approach has been used successfully in the field of solid state physics, for calculating the electronic structure of various materials. We will discuss these results in the next

section. Before that, we conclude our discussion of the self-consistent methods by indicating two possible extensions.

8.3.2 Beyond Hartree–Fock: inclusion of electron correlations

Clearly the HF approximation is too drastic and has to be improved by taking electron correlations into account. Atomic physicists have developed many methods to that effect, such as Configuration Interaction, the many-body perturbation theory, the R-matrix theory or the Multiconfiguration Hartree–Fock (MCHF) method [15]. Some of these methods are limited to correlations among discrete states, other ones include continuum states as well. In some cases at least (MCHF, for instance), the net result is to produce a wave function which is more concentrated around the origin, thus oscillates faster – and is therefore more likely to be well represented by wavelets. The computation usually requires a large number of terms. But again, considering the good localization properties of wavelets and their oscillatory behaviour, one may hope to reduce significantly the number of terms and accelerate the computation.

8.3.3 CWT realization of a 1-D HF equation

At the other extreme, a different wavelet method has been proposed recently [25] for studying the HF equation, albeit in a simplified one-dimensional version. The idea is to use the CWT in the same way as a Fourier or a Laplace transform, for obtaining a different realization of the differential equation to be solved.

One starts from the *radial* HF equation for the hydrogen atom, and extends it to $\mathbb{R}$ by antisymmetry, $x \mapsto -x$. Thus one obtains a 1-D differential equation:

$$-\frac{1}{2}f''(x) - \frac{f(x)}{|x|} = Ef(x), \quad f \in L^2(\mathbb{R}, dx). \tag{8.12}$$

Choosing as analysing wavelet the first derivative of a Gaussian, $w(x) \sim -x\,e^{-x^2/2}$, one takes the CWT of the two sides of (8.12), namely, with the usual notations ($a > 0, b \in \mathbb{R}$):

$$f(x) \mapsto \tilde{f}(a, b) \equiv \langle w_{ab} \mid f \rangle.$$

The result is a complicated integro-differential equation in the variables a and b, that one solves by iteration. The result is a marked improvement over the standard Slater or Gaussian inputs (the comparison is easy, since the exact

solution is known!). One may of course object that the situation treated in this model is too simplified and bears little resemblance to the real physical problem, but the idea looks nevertheless interesting.

As a final remark, we may note that the same authors [26] have also studied the 1-D HF equation (8.12) by expressing it into an orthonormal wavelet basis and applying the fast wavelet transform [14]. Again their results compare favourably with those of a Slater basis. Actually this technique of exploiting the fast convergence of the wavelet algorithm in HF calculations has been used by several authors, as we will see in Section 8.5.3.

8.4 Other applications in atomic physics

8.4.1 Combination of wavelets with moment methods

For concluding this survey of possible applications of wavelets to atomic physics, we discuss briefly a new method for calculating energy levels in atoms, based on a clever combination of the WT with the well-known method of moments [32, 33].

In the simplest case, consider a one-dimensional Schrödinger eigenvalue equation, with a potential $V(x)$:

$$-\frac{\mathrm{d}^2}{\mathrm{d}x^2}\Psi(x) + V(x)\Psi(x) = E\Psi(x). \tag{8.13}$$

The wavelet transform of $\Psi(x)$ with respect to the Mexican hat wavelet $\psi(x) = (1 - x^2)\exp(-1/2x^2)$ reads:

$$W\Psi(a, b) = Na^{-1/2}\int_{-\infty}^{+\infty} \Psi(x + b)\,(1 - (x/a)^2)\,e^{-x^2/2a^2}\,dx. \tag{8.14}$$

Introducing the moments

$$\mu_{b,\gamma}(p) \equiv \int_{-\infty}^{+\infty} x^p\,\Psi(x + b)\,e^{-\gamma x^2}\,dx,\ p \geq 0, \tag{8.15}$$

one may express the WT (8.14) as a linear combination of moments:

$$W\Psi(a, b) = N(2\gamma)^{1/4}[\mu_{b,\gamma}(0) - 2\gamma\mu_{b,\gamma}(2)], \quad \text{with } \gamma \equiv 1/2a^2. \tag{8.16}$$

On the other hand, these moments satisfy a first order differential equation in γ:

$$\frac{\partial}{\partial\gamma}\mu_{b,\gamma}(p) = -\mu_{b,\gamma}(p + 2). \tag{8.17}$$

The crucial point is that, if the potential $V(x)$ is a rational fraction (or may be transformed into one), then all the moments are linear combinations of the first $(1 + m_s)$ among them, the so-called initialization or missing moments. Inserting the corresponding expression into (8.17), one obtains a coupled set of linear differential equations in γ:

$$\frac{\partial}{\partial \gamma} \mu_{b,\gamma}(i) = \sum_{j=0}^{m_s} M_{ij}(\gamma, b, E)\, \mu_{b,\gamma}(j),\ 0 \leq i \leq m_s. \tag{8.18}$$

These equations may be integrated numerically, provided one has the value E of the ground state energy and the starting values $\mu_{b,0}(p)$, corresponding to the infinite scale limit $a = \infty$. Precisely, the Eigenvalue Moment Method (EMM), developed by Handy, Bessis and Morley [31], is able to give these initial data. Thus, the EMM yields the wavelet transform $W\Psi(a, b)$ of the unknown wave function $\Psi(x)$, which may then be obtained by a standard reconstruction formula (see Eq.(1.10) in Chapter 1, and more generally any textbook on wavelets, e.g. [19]).

This method, or variants thereof, has been applied in [32, 33] to the computation of energy levels and wave functions for a variety of one-dimensional potentials: the quartic anharmonic oscillator, the rational fraction $V(x) = gx^6(1 + \lambda x^2)^{-1}$, the Coulomb potential. In addition, the method probably extends to two or three dimensions. The results obtained in 1-D are reasonably good (the precision may be increased with more numerical effort), but, more important, this method introduces a totally new idea in the wavelet picture, which once again consists in combining wavelet techniques with existing methods. As such, this technique offers interesting perspectives for the future.

8.4.2 Wavelets in plasma physics

Since the physics of plasmas may be considered as a branch of atomic physics, it is appropriate to mention here an innovative application of the CWT to the analysis of intermittency in fusion plasmas [56]. Once again, the interesting methodological point is the combination of wavelet methods with a standard technique, in this case, bispectral methods. More precisely, the notion of bicoherence, which is a measure of the amount of phase coupling that occurs in the signal. Typically one studies the so-called wavelet bispectrum of a given signal $s(t)$, namely the function

$$B^W(a_1, a_2) = \int \overline{S(a, \tau)}\, S(a_1, \tau)\, S(a_2, \tau)\, d\tau, \tag{8.19}$$

the integral being taken over a finite time interval $\tau_1 \leq \tau \leq \tau_2$, and the following frequency sum rule holds

$$\frac{1}{a} = \frac{1}{a_1} + \frac{1}{a_2}. \tag{8.20}$$

The new point here consists in using the CWT of the signal in this definition, instead of its Fourier transform. Two remarks are in order here. First, this technique requires a complex wavelet, such as the Morlet wavelet, as always when phase information is essential. Second, the sum rule (8.20) can only be enforced if all frequencies are available, that is, if the continuous WT is used. Dyadic frequencies cannot in general satisfy the relation.

Using this tool in statistical analysis, one may detect the presence of intermittency and structure in the turbulent fusion plasmas [56]. A comprehensive description of this approach is contained in Chapter 6 of the present volume.

8.5 Electronic structure calculations

8.5.1 Principle

A basic problem in condensed-matter physics is the *ab initio* calculation of the electronic structure of a given material (ground state energy, wave function, etc.) Now, since the crystal is a 3-D periodic structure, it suffices to describe the electronic structure around a single lattice site and apply a Bloch transformation. Thus one comes back to the study of the electronic structure of a single atom or molecule, that is, to the problem discussed in Section 8.3. As explained there, the key is to find a good orthonormal basis, consisting of functions well adapted to the problem. Two standard methods are popular among chemists.

- *LCAO bases* (Linear Combination of Atomic Orbitals), based for instance on Slater or Gaussian orbitals. The method yields a good description of the electronic structure with relatively few terms, but it is difficult to improve it systematically (improving the LCAO method is sometimes described as an art!). In addition the expression for the forces is extremely complicated.
- *Plane wave bases*. These two difficulties disappear, but *a priori* plane waves are not suited for describing localized objects, since all information on space localization is lost. Yet the electronic structure of an atom is highly inhomogeneous in space, the wave function oscillates much more rapidly close to the nucleus. As a consequence a large number of terms is needed for describing the small inner region, but this increased precision is not necessary elsewhere.

In order to combine the advantages of the two methods, one should use a basis of localized functions, that allows to vary the precision according to the local electronic density. That suggests a wavelet basis, since wavelets are well localized, and adapt automatically to the scale of the object to be represented (the so-called automatic zoom effect). Several research groups have performed such an analysis, with different types of discrete wavelets, and we shall quickly review them.

8.5.2 A non-orthogonal wavelet basis

The first attempt [16] was based on a non-orthogonal multiresolution basis and its approximation by Gaussians and Mexican hats. The idea is to consider a multiresolution scale in three dimensions, $\{V_j; j \in \mathbb{Z}\} \subset L^2(\mathbb{R}^3)$, as described in Chapter 1, Section 1.3, but *without* the assumption of orthogonality:

$$V_{j+1} = V_j \dot{+} W_j, \tag{8.21}$$

where $\dot{+}$ denotes a direct sum, not necessarily orthogonal (hence the decomposition in (8.21) is still unique). The interpretation is the usual one: V_j describes the approximation at resolution 2^j, and W_j the additional details needed for passing from the resolution 2^j to the finer resolution 2^{j+1}. Thus one gets, as in Eq.(1.17):

$$L^2(\mathbb{R}^3) = V_{j_o} \dot{+} \left(\sum_{j \geq j_o} W_j \right), \tag{8.22}$$

where j_o corresponds to the lowest resolution considered and $\sum$ denotes again a direct sum. Then one chooses two orthogonal bases, localized around the nodes of a fixed 3-D lattice:

$$\{\phi_{j\mathbf{n}}(\mathbf{r})\} \in V_j \quad \text{and} \quad \{\psi_{j\mathbf{n}}(\mathbf{r})\} \in W_j, \tag{8.23}$$

where $\mathbf{n}$ denotes a lattice point and $j \in \mathbb{Z}$. From (8.22), the practical expansion of a general wave function into these bases reads:

$$f(\mathbf{r}) = \sum_{\mathbf{n}} a_{j_o\mathbf{n}} \phi_{j_o\mathbf{n}}(\mathbf{r}) + \sum_{j=j_o}^{j_{max}} \sum_{\mathbf{n}} d_{j\mathbf{n}} \psi_{j\mathbf{n}}(\mathbf{r}) \tag{8.24}$$

In this truncated expansion, $\phi_{j_o\mathbf{n}}$ is a scaling function, $\psi_{j\mathbf{n}}$ is a wavelet, both centred around the lattice point $\mathbf{n}$, and j_{max} is the finest resolution, corresponding to the desired precision. This expansion still has an infinite number of terms, since $\mathbf{n}$ runs over the whole lattice. However, both $\phi_{j\mathbf{n}}$ and $\psi_{j\mathbf{n}}$ are

supposed to be well localized, so one has to keep only those functions which have significantly large coefficients $a_{j_o\mathbf{n}}$, resp. $d_{j\mathbf{n}}$, for the problem at hand. This means that one allows different resolutions for different localized regions. In particular, since the electronic wave function oscillates more rapidly in the atomic core region, one should add higher resolution scales j in the core region, where the precision must be higher, but only there. Globally the number of terms is thus considerably reduced.

The technique introduced in [16] for practical calculations runs as follows.

- One starts at resolution $j_o = 0$ with a cubic lattice L_0, of lattice spacing d_o small enough (the final basis should be a sufficiently tight frame). Then, for each resolution $j = 1, 2 \ldots, j_{max}$, one considers the refined lattice L_j of spacing $2^{-j}d_o$. The successive basis functions will be localized on the nodes of the finest lattice $L_{j_{max}}$, with no overlap between different resolutions. Notice that this lattice is fixed in space, independently of the position of the atomic nuclei.
- In order to adapt the resolution to the electronic density, one draws around each nucleus a sequence of concentric spheres S_j of radii $r_j = 2^{-j}r_0$, $j = 0, \ldots, j_{max}$. Then the finite (approximate) basis consists of the following functions: (i) scaling functions $\phi_{0\mathbf{n}}$ centred on the nodes of L_0 localized inside S_0; (ii) wavelets $\psi_{0\mathbf{n}}$ on the nodes of L_0 localized inside S_1, (iii) wavelets $\psi_{1\mathbf{n}}$ on the nodes of $L_1 \setminus L_0$ localized inside S_2; and so on until $j = j_{max}$. This arrangement is schematized in Figure 8.10 in a 2-D version.

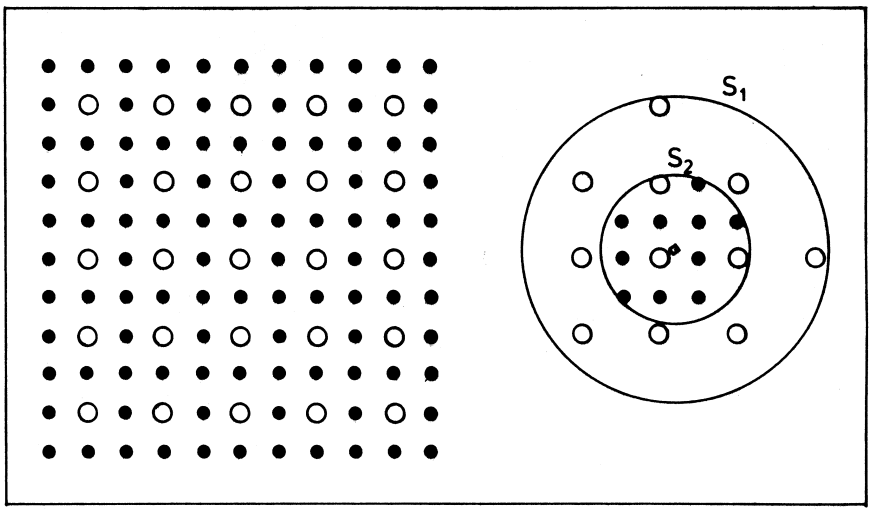

Fig. 8.10. The geometrical arrangement of [16] in a 2-D version. (left) The lattice L_0, corresponding to the resolution $j = 0$ (open circles) and the nodes of $L_1 \setminus L_0$, corresponding to $j = 1$ (black circles). (right) The spheres S_1 and S_2, both centred on an atomic nucleus (lozenge), and containing centres of wavelets with $j = 0$ and $j = 0, 1$, respectively.

The net result is a highly flexible finite basis, with higher resolutions introduced only where they are needed, namely close to the nuclear cores.

The next problem is to choose basis functions which are both efficient and simple to work with. Cho *et al.* [16] use Gaussians for $\phi_{0,\mathbf{n}}$ and Mexican hat wavelets for $\psi_{j,\mathbf{n}}$. Strictly speaking, this choice is not allowed, since these functions do not generate an orthogonal basis, but only a tight frame [19]. However they give an extremely good approximation to such a basis, as results from the following argument [9].

The crucial input in the construction of a wavelet basis is the pair m_0, m_1 of 2π-periodic functions defining the two-scale relations, for the scaling function and the wavelet, respectively (see [19] and Chapter 1, section 1):

$$\widehat{\phi}(2\omega) = m_0(\omega)\widehat{\phi}(\omega), \quad \widehat{\psi}(2\omega) = m_1(\omega)\widehat{\phi}(\omega) \tag{8.25}$$

(in the orthogonal case, one usually takes $m_1(\omega) = \overline{m_0(\omega+\pi)}e^{i\omega}$). According to [17, Theorem 5.16], the decomposition (8.21) is unique (but without orthogonality in general) iff

$$m_0(\omega)m_1(\omega+\pi) - m_1(\omega)m_0(\omega+\pi) \neq 0, \quad \text{for all } \omega \in [0, 2\pi). \tag{8.26}$$

Cho *et al.* [16] choose the following functions :

$$m_0(\omega) = \sum_{j\in\mathbb{Z}} \exp\left(-\frac{3}{2}\sigma^2(\omega - 2\pi j)^2\right),$$

$$m_1(\omega) = -e^{i\omega}\left(\omega - 2\pi\left[\frac{\omega+\pi}{2\pi}\right]\right)^2 m_0(\omega),$$

where [.] denotes the integer part function. It is readily seen by direct computation that these functions satisfy the criterion (8.26), thus guaranteeing a unique decomposition (8.21). Furthermore, and this is the interesting point, for $\sigma = 1.35$, m_0 and m_1 generate a scaling function $\phi(x)$ and a 'wavelet' $\psi(x)$ that match, respectively, a Gaussian $G(x)$ and a Mexican hat $-G''(x)$ within an absolute error of 10^{-10}. This is indeed a good approximation, which tends to confirm the practical efficiency of the tight frame based on the Mexican hat wavelet.

As a test, the method is applied to the hydrogen atom [16]. The best result is that the (known) ground state radial wave function is reproduced within 0.3% with an 85 function basis ($j_{max} = 1, r_o = 2$ a.u.). What is more convincing, the ground state energies of all elements, from hydrogen to uranium, may be estimated within 3% using a single 67 function basis, with $j_{max} = 10$. Next the total energy of a hydrogen molecular ion H_2^+ is calculated as a function of the separation R between the two protons. With a basis of 141 to 167 functions (depending on R), the exact values are reproduced within

1%. Finally, the analysis is extended [8] to the full carbon atom, in the local density approximation [37], and it yields again rather accurate energies and wave functions.

The conclusion is that a (quasi-)wavelet basis offers a very good alternative to standard methods for calculating the electronic structure of atoms or molecules, because it allows to vary the spatial resolution with space, contrary to the LCAO or plane wave methods. The analysis extends immediately to periodic systems by introducing a Bloch transformation. But, of course, the precision obtained in this approach is not entirely satisfactory.

One reason is the conflict between the spherical geometry of the atom and the Cartesian geometry of the lattice used in the wavelet expansion. Some progress in this direction has been made in the recent work of the MIT group [10], with a more isotropic scheme based on the so-called *interpolets* and combining wavelets with finite element methods (see also [7]). Another improvement, due to the same group, consists of combining wavelets with traditional multigrid methods, which also allow to vary the spatial resolution. Thus once again, the lesson is that wavelets yield optimal results when they are combined with standard methods, well adapted to the problem at hand (and usually the result from a long practice).

8.5.3 Orthogonal wavelet bases

Instead of the non-orthogonal scheme of [16], several groups have considered genuine orthonormal wavelet bases, e.g. Daubechies or Meyer bases. Once again, the key to efficiency lies in a clever selection of the most significant expansion coefficients.

8.5.3.1 Diagonalizing the LDA Hamiltonian in a Daubechies basis

Wei and Chou [57] essentially diagonalize the Hamiltonian in the local density approximation (LDA [37]), based on the Kohn–Sham equation (instead of the Schrödinger equation) :

$$\left(-\frac{\hbar^2}{2m}\Delta + V[\mathbf{r};\,\rho(\mathbf{r})]\right)\psi_n(\mathbf{r}) = \epsilon_n\psi_n(\mathbf{r}), \tag{8.27}$$

where $\rho(\mathbf{r}) = \sum_n f_n|\psi_n(\mathbf{r})|^2$ is the local electronic density and $V[\mathbf{r};\,\rho(\mathbf{r})]$ an effective potential. The idea is to expand the solution of the effective equation (8.27) in a suitable wavelet basis, so as to get a small number of significant coefficients (the same numerical exigence underlies the solution of the Schrödinger equation described in Section 8.2). The authors of [57] choose a Daubechies D6 wavelet basis of compact support, which generates a 3-D

orthonormal basis by a threefold tensor product. Physical quantities are then calculated in this basis, using fast wavelet transform algorithms. For instance, they evaluate matrix elements of the Hamiltonian, $\int \psi_l H \psi_m d^3x$, where ψ_l stands for the wavelet basis vectors, and in particular potential terms $\int \psi_l U \psi_m d^3x$, where U may be a local potential (ionic, Hartree or exchange-correlation) or a nonlocal separable pseudopotential. The grid is the standard multiresolution grid, and its position relative to the centres of the atoms is essentially irrelevant. As compared to [16], no artificial cutoff is put by hand, the rapid convergence of the calculation follows from the smallness of the compact support of the D6 wavelet, which yields sparse matrices.

With this technique, one computes [57] the total energies for a (fictitious) hydrogen atom and for a dimer molecule, H_2 or O_2 (as a function of the bond length). In all cases, the method requires relatively few basis functions (1000 or 2000) as compared to the plane wave method ($\sim$ 8700), with similar results. Thus it offers hope for a serious improving of standard calculations. One may remark, however, that the plane wave calculation that serves for comparison has not been optimized (for instance, the energy cutoff of 100 Ry on the pseudopotential is abnormally high, and thus leads to a larger number of terms than necessary), so that the improvement reported may be smaller than claimed. Also the case of small diatomic molecules is specially unfavourable for a plane wave basis (too much void in the supercell). It is plausible that the two methods would have similar performances for larger molecules [28].

8.5.3.2 Molecular dynamics algorithm in a Daubechies basis

Tymczak and Wang [55] also use a 3-D Daubechies wavelet basis for performing electronic structure calculations in a local density approximation, starting again from the Kohn–Sham equation (8.27). However, instead of trying to squarely diagonalize the Kohn–Sham Hamiltonian in the wavelet basis, as the previous authors, they resort to a standard algorithm of molecular dynamics (Car–Parrinello) to obtain the eigenfunctions iteratively (this algorithm is similar to the dynamic simulated annealing method familiar in statistical mechanics). Of course, as in the other approaches, the key point for combining speed and precision of the calculation is to select adequately the most significant wavelet coefficients to be kept. In order to do so, one may exploit the self-similar behaviour of wavelet coefficients: from each scale to the next finer one, all coefficients are multiplied by a common small factor (which gets smaller for an increasing number of vanishing moments of the wavelet). Hence those coefficients that are negligible at a given scale lead to negligible ones at finer scales, no significant coefficients reemerge. Then,

combining the selection of significant wavelet coefficients and the Car–Parrinello algorithm at each successive scale, from coarse to fine, one obtains fast convergence to the approximate eigenvalues and reasonably good values for the latter. Both the convergence and the compression rates (percentage of coefficients being kept) increase with the grid size, and so does the advantage of the method over the conventional plane wave approach. Only simple systems are treated in [55], namely the 3-D harmonic oscillator, the hydrogen atom, and the LDA to the helium atom and the hydrogen dimer H_2. However, the method seems powerful enough for attacking real multi-electron systems.

8.5.3.3 Galerkin method in a Meyer basis

Yamaguchi and Mukoyama [58] solve the *radial* Schrödinger equation by a variational (Galerkin) method, using an effective one-electron local potential and extending the equation to $\mathbb{R}$ by antisymmetry $x \mapsto -x$, as in Section 8.3.3. In order to formulate the variational equations (see Section 8.3), they expand the wave function into an antisymmetrized Meyer wavelet basis (C^∞, symmetric, all moments vanishing, but noncompact support), keeping only the most significant terms, as usual. By this technique they compute energy eigenvalues and wave functions for hydrogen, neon and argon atoms, and continuum wave functions (corresponding to pseudostates) for the argon atom. As a test of the numerical quality of their wave functions, they calculate, respectively, radiative transition rates in neon and argon atoms, and partial photoionization rates for an argon atom in its 1s, 2s and 3s state. The results are in excellent agreement with those obtained by the traditional Hartree–Fock–Slater method. However, one may notice that a large number of basis vectors is necessary for a good precision (475 for Ar), especially for the excited states (3s, 3p), which are much less localized.

An interesting remark is that each type of atomic state (lower bound state, Rydberg state, continuum state) has a characteristic distribution in the wavelet parameter space. This permits one to choose for each kind of physical process an adequate trial function before performing the variational procedure.

8.5.4 Second generation wavelets

The Daubechies wavelets used in [55] and [57] have compact support, which is numerically convenient, but they are not very smooth, and this becomes a drawback when it comes to solving differential equations, for instance diagonalizing a Laplacian. An elegant way of avoiding this problem is to use

biorthogonal wavelets, which offer the most flexible version of wavelet techniques, and are also the most widely used in the wavelet community.

In the case of quantum physics applications, this step was made very recently in a paper by Goedecker and Ivanov [27], in which they treat the full Coulomb problem by pure wavelet methods. Namely they solve the Poisson equation $\Delta V = 4\pi\rho$, by expanding both the potential V and the electronic density ρ in a biorthogonal basis, in the present case a second generation wavelet basis (8th order lifted Lazy wavelet) [53]. Varying the resolution according to the electronic density, as in [16], and using BCR fast wavelet algorithms [14], they obtain rather spectacular results, definitely improving upon [57]. For instance, they are able to treat the potential arising from a fully 3-D all-electron uranium dimer. To give an idea of the power of the method, this problem involves length scales that differ by more than 3 orders of magnitude, and so does the potential. The resolutions involved differ by 7 orders of magnitude, and the potential is obtained with 6 significant digits throughout the whole region. As far as we know, this is the most successful application so far of wavelet methods in an atomic structure calculation.

8.6 Wavelet-like orthonormal bases for the lowest Landau level

As mentioned already, the electronic structure calculations described in the previous section give information on the bulk properties of solids, via a Bloch transformation [10]. Besides these calculations, wavelets have found applications in two other problems of condensed-matter physics.

The first one is a striking similarity between wavelets and Wannier functions of a 1-D crystal [35]. The context is the study of *inflation*, which means the following. Any one-dimensional periodic system of period a may be viewed as a $2a$-periodic system. The question is, how does the dynamics change? In particular, how do Bloch and Wannier functions transform under inflation? It turns out that both types of functions obey two-scale relations, characteristic of multiresolution wavelets [17, 19]. In particular, the Wannier functions of a free electron in the 1-D periodic system coincide with the Littlewood–Paley wavelets (see Section 8.6.3.2). It remains to be seen whether this is a mere curiosity or physically useful information.

The other application pertains to a 2-D electron gas submitted to a strong magnetic field, that is, the system in which the Quantum Hall Effects (integer or fractional) take place. We will devote the rest of this section to this problem and the promising role of wavelets in that context.

8.6.1 The Fractional Quantum Hall Effect setup

The system considered in the Fractional Quantum Hall Effect (FQHE) is a (quasi)-planar gas of electrons in a strong magnetic field perpendicular to the plane (see [48] for a review and the original references). The first problem to tackle is to find the ground state of the system. As in the electronic structure calculations described in Section 8.5, the key physical parameter is the electron density, which is measured by the so-called *filling factor* ν. As shown in [11], good energy values are obtained for small ($0 < \nu < \frac{1}{5}$) or high ($\frac{4}{5} < \nu < 1$) electron densities with a Hartree–Fock description of a system of N two-dimensional electrons.

The first step in the HF procedure is to select an adequate wave function for a single electron in the magnetic field. As it is well known [48], the energy levels, the so-called Landau levels, are infinitely degenerate, and there arises the problem of finding a good basis in the corresponding Hilbert subspace. In particular, the ground state belongs to the lowest Landau level (LLL). A general method has been proposed for constructing an orthogonal basis for the LLL, starting from standard 1-D orthogonal wavelet bases [2, 12, 13]. We will describe this construction below, but we shall first recall the physical background of the problem.

Consider a single electron confined in the xy-plane and subjected to a strong magnetic field in the z-direction. In the symmetric gauge, the Hamiltonian reads (we use units such that $\hbar = M = e|\vec{H}|/c = 1$):

$$H_o = \frac{1}{2}(p_x - y/2)^2 + \frac{1}{2}(p_y + x/2)^2. \tag{8.28}$$

Introducing the canonical variables

$$P' = p_x - y/2, \quad Q' = p_y + x/2, \tag{8.29}$$

this can be written in the form of the Hamiltonian of a harmonic oscillator:

$$H_o = \tfrac{1}{2}(Q'^2 + P'^2). \tag{8.30}$$

Therefore the eigenstates of the Hamiltonian (8.28) can be found explicitly, and they have the following form:

$$\Phi_{mn}(x, y) \sim e^{(x^2+y^2)/4}(\partial_x + i\partial_y)^m\,(\partial_x - i\partial_y)^n e^{-(x^2+y^2)/2},\ m, n = 0, 1, 2, \ldots, \tag{8.31}$$

corresponding to the eigenvalues $E_{mn} \equiv E_n = n + 1/2$. Thus the energy levels are all degenerate in m, so that the ground level (LLL) is spanned by the set $\{\Phi_{m0}(x, y)\}$, which forms an orthonormal basis. However these wave func-

tions are not very well localized, since the mean value of the distance from the origin, $r \equiv \sqrt{x^2 + y^2}$, increases with m. Yet the physics of the problem requires that the wave functions be fairly well localized, since the system tends, as $T \to 0$, to the configuration of the Wigner crystal, that is, a triangular lattice [11]. Thus the basis $\{\Phi_{m0}(x, y)\}$ of the LLL is inadequate for the present purposes.

8.6.2 The LLL basis problem

In order to find another basis of eigenfunctions, orthogonal or not, spanning the same energy level, one may use the method introduced in [11], which is based on a technique introduced by Moshinsky and Quesne [49]. The transformation (8.29) can be seen as a part of a canonical transformation from the variables x, y, p_x, p_y into the new ones Q, P, Q', P', where

$$P = p_y - x/2, \quad Q = p_x + y/2. \tag{8.32}$$

These operators satisfy the following commutation relations:

$$[Q, P] = [Q', P'] = i, \tag{8.33}$$

$$[Q, P'] = [Q', P] = [Q, Q'] = [P, P'] = 0. \tag{8.34}$$

Then a wave function in the (x, y)-space is related to its PP'-expression by the formula

$$\Phi(x, y) = \frac{e^{ixy/2}}{2\pi} \iint_{\mathbb{R}^2} e^{i(xP' + yP + PP')} \Psi(P, P')\, dP dP'. \tag{8.35}$$

In virtue of the expression (8.30) of H_o, the Schrödinger equation $H_o\Psi = \frac{1}{2}(Q'^2 + P'^2)\Psi = E\Psi$ admits factorized solutions $\Psi(P, P') = f(P')h(P)$. Thus the ground state wave function of (8.30) must have the form

$$\Psi_0(P, P') = f_0(P')h(P), \tag{8.36}$$

where $f_0(P') = \pi^{-1/4} e^{-P'^2/2}$, and the function $h(P)$ is arbitrary, which manifests the infinite degeneracy of the LLL.

Depending on the choice of $h(P)$, several types of bases for the LLL may be obtained, according to the following general scheme. Inserting (8.36) into the integral (8.35), the Gaussian integration on P' can be performed exactly. Next, taking a wave function $\Psi_n(P, P') = f_0(P')\, h_n(P)$, where $\{h_n(P)\}$ is an arbitrary basis in $L^2(\mathbb{R})$, we define:

$$h_n^{(2)}(x, y) = \frac{e^{ixy/2}}{\sqrt{2}\pi^{3/4}} \int_{-\infty}^{\infty} e^{iyP} e^{-(x+P)^2/2}\, h_n(P)\, dP. \tag{8.37}$$

Then the set $\{h_n^{(2)}(x, y)\}$ is a basis for the LLL, and it is orthonormal iff $\{h_n(P)\}$ is orthonormal in $L^2(\mathbb{R})$. This follows from the canonicity of the change of variables given in Eqs. (8.29), (8.32) or simply by an explicit calculation of the matrix element $\langle h_n|h_m\rangle$, using the integral (8.37). Several examples of this construction have been presented in the literature.

(1) Bagarello *et al.* [11] choose for the ground state a Gaussian $h_0(P) = f_0(P)$, which yields, by (8.37), $h_0^{(2)}(x, y) = \Phi_{00}(x, y) \sim \exp -(x^2 + y^2)/4$. Then they construct a complete set of basis functions of the LLL by acting on $\Phi_{00}(x, y)$ with the so-called magnetic translation operators. The resulting basis vectors have Gaussian localization around the sites of a regular two-dimensional lattice, and thus the basis is lattice-translation invariant. However, each vector has a well-defined, fixed (essential) support, so that there is no possibility of modifying the mutual overlap for fixed electron density. In addition, this basis is not orthogonal, since coherent states are in general not mutually orthogonal. Enforcing orthogonality (by the Gram–Schmidt method, for instance) spoils much of the simplicity of the basis functions, and in particular the localization properties for intermediate fillings and the lattice-translation invariance property.

(2) In order to keep the good localization properties and some sort of translation invariance, Ferrari [23] has constructed an orthonormal basis for the LLL by taking infinite superpositions of the above (coherent) states. The resulting basis vectors are Bloch functions, which may be made translation invariant over the nodes of a given lattice, typically triangular or hexagonal (remember that the Wigner crystal is a triangular lattice). Clearly this basis describes very well the two-dimensional low-density system of electrons of the FQHE, but its construction is rather involved and ad hoc.

(3) Since one wants basis wave functions which are both well localized *and* orthogonal, obvious candidates are orthogonal wavelets. They do enjoy good localization properties, and the latter are easily controlled by varying the scale parameter, in contrast to the Gaussian-like functions of [11]. In addition, the physical problem has an intrinsic hierarchical structure [29, 30]. In particular, the filling factor may take arbitrary rational values, and this suggests a fractal behaviour, as remarked recently [47]. All this points again to wavelets. In the next section, we will review several examples of this construction, as proposed in [2, 12, 13].

8.6.3 Wavelet-like bases

8.6.3.1 The Haar basis

Let us look first at the LLL basis generated by the Haar wavelet basis [19]. Since the mother wavelet $h(x)$ is a discontinuous function, its localization in

frequency space is poor, it decays as ω^{-1}. However, the transformation (8.37) is not a Fourier transform, hence it is not clear *a priori* that the corresponding functions $\{h_{jk}^{(2)}(x, y)\}$ will also have a poor localization in both variables. In fact it is *not* the case, as can be seen by investigating the asymptotic behaviour of the basis functions.

Using standard results on Gaussian integrals, one finds for the ground state wave function:

$$H_{00}(x, y) = \frac{e^{-ixy/2} e^{-y^2/2}}{2\pi^{1/4}} \{2\,\Xi(x - iy + 1/2) - \Xi(x - iy) - \Xi(x - iy + 1)\}, \tag{8.38}$$

where

$$\Xi(z) = \operatorname{erf}(z/\sqrt{2}) = \frac{2}{\sqrt{\pi}} \int_0^{z/\sqrt{2}} e^{-t^2}\, dt, \quad z \in \mathbb{C}.$$

Using the asymptotic expansion of the error function, we get, for $|x|, |y| \gg 1$:

$$H_{00}(x, y) \simeq \frac{e^{ixy/2} e^{-x^2/2}}{2\pi^{1/4}} \sqrt{\frac{2}{\pi}} \left(\frac{1}{x - iy} + \frac{e^{-1/2 - x + iy}}{x - iy + 1} - 2 \frac{e^{-1/8 - (x - iy)/2}}{x - iy + 1/2} \right), \tag{8.39}$$

which displays the Gaussian localization of the wave function in the variable x and the rather poor one in y (decay as y^{-1}). This behaviour is confirmed in Figure 8.11 (left), which shows the modulus of $H_{00}(x, y)$ in a 3-D perspective. Clearly the function $H_{00}(x, y)$ is much better localized in the x variable than in y.

An analogous behaviour can be obtained for the generic function $H_{jk}(x, y)$, which may also be calculated exactly. Using (8.37), it is easily seen that the asymptotic behavior of $h_n^{(2)}(x, y)$ in x is governed by the asymptotic behaviour of $h_n(P)$, and the one in y by that of the Fourier transform of $h_n(P)$. Since in the present case, $h_{jk}(P)$ has compact support, we expect $H_{jk}(x, y)$ to be strongly localized in x and delocalized in y, and that its decay in x gets faster for smaller j. This is indeed the case, as may be seen on the figures presented in [12].

8.6.3.2 The Littlewood–Paley and other wavelet bases

Another simple example of an orthonormal wavelet basis in $L^2(\mathbb{R})$, also coming from MRA, is the Littlewood–Paley basis [19], generated from the mother wavelet

$$\Psi(x) = (\pi x)^{-1}(\sin 2\pi x - \sin \pi x). \tag{8.40}$$

The behaviour of this function is complementary to that of the Haar wavelet: it has a compact support in frequency space but it decays like $1/x$ in configuration space.

An analogous complementary behaviour is found also for the corresponding LLL wave functions. They are exponentially localized in the y-variable, while in the other variable they behave like $1/x$. This is manifest on the asymptotic behaviour of $\Psi_{00}(x, y)$ for $|x|, |y| \gg 1$. By the same method as before, one finds:

$$\Psi_{00}(x, y) \simeq \frac{e^{-ixy/2}e^{-y^2/2}}{2\pi^{5/4}} \left\{ -\frac{e^{2\pi(y+ix)}e^{-2\pi^2}}{|2\pi - y - ix|} + \frac{e^{\pi(y+ix)}e^{-\pi^2/2}}{|\pi - y - ix|} - \frac{e^{-2\pi(y+ix)}e^{-2\pi^2}}{|2\pi + y + ix|} + \frac{e^{-\pi(y+ix)}e^{-\pi^2/2}}{|\pi + y + ix|} \right\}, \tag{8.41}$$

which displays the exponential decay of $|\Psi_{00}(x, y)|$ in y and the slow decay in x, as observed in Figure 8.11 (right).

Similar considerations can be made for the LLL bases obtained by (8.37) from other 1-D wavelet orthonormal bases; for instance [12], the following.

- The *Journé basis*, which does not come from MRA (see [19], p. 136). This case is very similar to the Littlewood–Paley basis, since here too the mother wavelet has compact support in frequency space.
- *Spline bases*, for instance the order 1 splines, coming from the triangle or 'tent' function as scaling function.

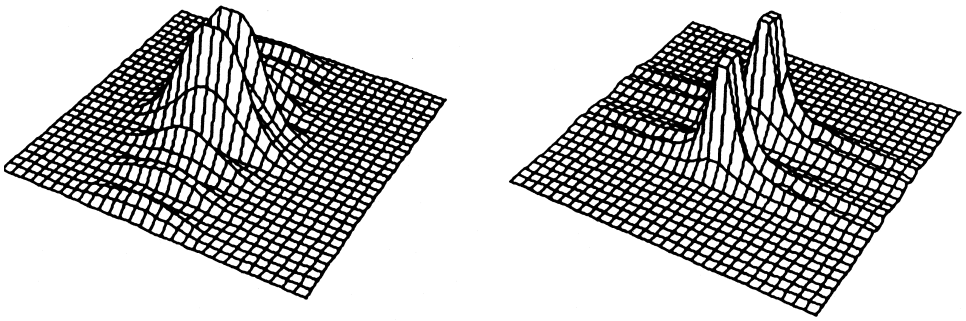

Fig. 8.11. 3-D perspective view of the modulus of the lowest LLL basis functions; the x-axis runs from left to right, the y-axis from front to back. (Left) The Haar function $H_{00}(x, y)$. (Right) The Littlewood–Paley function $\Psi_{00}(x, y)$.

8.6.3.3 Outcome

In conclusion we may say that the orthonormal bases obtained so far are not yet sufficient for a good solution of the LLL problem, except at very low electron density. However, the construction sketched above suggests a general method for designing good bases, with localized functions and respecting the symmetry of a given lattice, for instance, a triangular lattice. This goes in the right direction, since the whole QHE may be characterized as the transport of electrons in a (local) Wigner crystal [47]. The most promising point of such wavelet bases is the possibility of controlling the width of the (essential) supports, hence the overlap between basis functions at neighbouring points, with help of the scaling parameter.

8.6.4 Further variations on the same theme

In a further paper, Bagarello [13] has investigated another aspect of the trial wave function introduced in [11] for a two-dimensional system of electrons in Coulomb interaction. Namely he compares the ground state energy given by harmonic oscillator wave functions with that obtained with particular wavelets. It turns out that the latter always give results that can easily be interpreted as localization properties of the wave function.

Consider an N-electron system in $\mathbb{R}^2$, with Hamiltonian

$$H = \sum_{i=1}^{N} H_o(i) + \frac{1}{2}\sum_{i\neq j} \frac{1}{|\mathbf{r}_i - \mathbf{r}_j|} \tag{8.42}$$

$$H_o = \frac{1}{2}(p_x^2 + x^2) + \frac{1}{2}p_y^2 + p_x p_y. \tag{8.43}$$

Then, under the following canonical transformation:

$$\begin{array}{rclcrcl} Q &=& p_x + p_y, & & P &=& -x, \\ Q' &=& p_y, & & P' &=& x - y, \end{array} \tag{8.44}$$

the free Hamiltonian turns into that of a harmonic oscillator, as before:

$$H_o = \tfrac{1}{2}(Q^2 + P^2), \tag{8.45}$$

and again one has an integral transform relating the QQ' wave function to the original one:

$$\Psi(x, y) = \frac{1}{2}\iint_{\mathbb{R}^2} e^{i[Q'(x-y)+Qx]}\, \Phi(Q, Q')\, dQ\, dQ'. \tag{8.46}$$

Here also the free Schrödinger equation admits factorized solutions

$$\Phi(Q, Q') = \pi^{-1/4}\, e^{-Q^2/2}\, \phi(Q'), \tag{8.47}$$

where $\phi(Q')$ is an arbitrary function. Choosing for the latter various basis functions, such as elements of the Littlewood–Paley, Haar or harmonic oscillator basis, one may compute the ground state energy E_c of the N-electron system, with the wave function taken again as a Slater determinant, in the familiar Hartree–Fock manner. Actually E_c is the sum of two terms, the direct one and the exchange term (see Section 8.3.1), but the latter is much smaller and may be neglected. As a preparation for the FQHE, one should also consider the electrons localized on the nodes of a lattice generated by magnetic translations, as explained in the preceding section.

Calculations of this type are presented in [13] for $N = 2$ (this case already displays the general features) and several configurations. For instance, two electrons localized at the origin (with different wave functions, otherwise the Slater determinant would vanish identically); or two electrons on the y-axis, separated by a magnetic translation. In both cases, the value obtained for the energy of the trial ground state shows that the wavelet wave function is better localized than the harmonic oscillator wave function.

All these results strongly suggest that wavelet bases, localized around the nodes of the triangular Wigner crystal, may be extremely useful for finding the ground state wave function of the FQHE.

8.7 Outcome: what have wavelets brought to us?

Looking in retrospect at the discussion above, we may conclude that wavelets can be used profitably in various problems in atomic physics and in solid state physics, under different aspects and for different purposes. For instance, we may state the following.

- The detailed description and physical understanding of harmonic generation (and similar transient phenomena) is inaccessible to standard spectral methods, it requires a *time–frequency representation*, by wavelets or Gabor analysis.
- The computation of N-electron atomic wave functions (HF and relatives) demands a good *orthogonal basis* on the half line $\mathbb{R}^+$, and a wavelet basis seems well-adapted.
- Finally, there is the possibility of using 2-D orthogonal wavelet bases for the description of 2-D phenomena in solid state physics, such as the FQHE.

In all these applications, the key property of wavelets is their good localization, both in space and in frequency, and the possibility of controlling it by scaling (the automatic zooming property). This property permits, for instance, to vary the precision of electronic structure calculations in space,

depending on the value of the local electronic density. The net result is a reduction of the number of terms required for the expansion of wave functions in the chosen bases. This is analogous to the higher compression rates achieved with wavelet bases in the synthesis and transmission of signals.

As a final point, we may remark that all the applications described in this chapter consider the WT as a mathematical tool, whereas wavelets might also be used as genuine physical entities, exactly as coherent states – which they are after all! Many interesting phenomena could be described in that language (Rydberg atoms, semiclassical limit, revivals, . . .). Finally there is also the possibility to use different wavelets, such as the CS associated to the Schrödinger group [22].

Our conclusion will be that the applications of wavelets in atomic physics and in solid state physics are a new field (it is characteristic that most of the papers quoted in this chapter have appeared in the past two years). Many promising results have been obtained already, much work remains to be done, and hopes for progress are reasonably well-founded. In addition, it is likely that new applications in various domains of quantum (or classical) physics will be found in the near future.

Acknowledgements

It is a pleasure to thank T.A. Arias for communicating additional information about his work, and Z. Felfli, X. Gonze, C. Handy, R. Murenzi, B. Torrésani, C.J. Tymczak and X.Q. Wang for interesting discussions and comments about several aspects of this chapter.

References

[1] S.T. Ali, J.-P. Antoine, J.-P. Gazeau and U.A. Mueller, Coherent states and their generalizations: A mathematical overview, *Reviews Math. Phys.*, **7**: 1013–1104, (1995)

[2] J.-P. Antoine and F. Bagarello, Wavelet-like orthonormal bases for the lowest Landau level, *J. Phys. A: Math. Gen.*, **27**: 2471–2481, (1994)

[3] Ph. Antoine, B. Piraux and A. Maquet, Time profile of harmonics generated by a single atom in a strong electromagnetic field, *Phys. Rev. A*, **51**: R1750–R1753, (1995)

[4] Ph. Antoine, B. Piraux, D.B. Milošević and M. Gajda, Generation of ultrashort pulses of harmonics, *Phys. Rev. A*, **54**: R1761–R1764, (1996)

[5] Ph. Antoine, A. L'Huillier and M. Lewenstein, Attosecond pulse trains using high-order harmonics, *Phys. Rev. Lett.*, **77**: 1234–1237, (1996)

[6] Ph. Antoine, B. Piraux, D.B. Milošević and M. Gajda, Temporal profile and time control of harmonic generation, *Laser Physics*, **7**: 594–601, (1997)

[7] Proc. March 1996 Meeting of the Amer. Phys. Soc., Session R19, *Bull. Amer. Phys. Soc.*, **41**: 746–748, (1996)
[8] T.A. Arias, K.J. Cho, P.K. Lam, J.D. Joannopoulos and M.P. Teter, Wavelet-transform representation of the electronic structure of materials, in *Toward Teraflop Computing and New Grand Challenge Applications*, p. 23; ed. P.K. Kalia and P. Vashishta (Nova Scient. Publ., 1995)
[9] T.A. Arias, private communication
[10] T.A. Arias, http://web.mit.edu/muchomas/www/home.html
[11] F. Bagarello, G. Morchio and F. Strocchi, Quantum corrections to the Wigner crystal: A Hartree–Fock expansion, *Phys. Rev. B*, **48**: 5306–5314, (1993)
[12] F. Bagarello, More wavelet-like orthonormal bases for the lowest Landau level: some considerations, *J. Phys. A: Math. Gen.*, **27**: 5583–5597, (1994)
[13] F. Bagarello, Applications of wavelets in quantum mechanics: a pedagogical example, *J. Phys. A: Math. Gen.*, **29**: 565–576, (1996)
[14] G. Beylkin, R. Coifman and V. Rokhlin, Fast wavelet transforms and numerical algorithms, *Comm. Pure Appl. Math.*, **44**: 141–183, (1991)
[15] B.H. Bransden and C.J. Joachain, *Physics of Atoms and Molecules* (Longman, London and New York, 1983)
[16] K. Cho, T.A. Arias, J.D. Joannopoulos and P.K. Lam, Wavelets in electronic structure calculations, *Phys. Rev. Lett.*, **71**: 1808–1811, (1993)
[17] C.K. Chui, *An Introduction to Wavelets* (Academic Press, San Diego, 1992)
[18] P.B. Corkum, Plasma perspective on strong-field multiphoton ionization, *Phys. Rev. Lett.*, **71**: 1994–1997, (1993)
[19] I. Daubechies, *Ten Lectures on Wavelets* (SIAM, Philadelphia, PA, 1992)
[20] N. Delprat, B. Escudié, Ph. Guillemain, R. Kronland-Martinet, Ph. Tchamitchian and B. Torrésani, Asymptotic wavelet and Gabor analysis: Extraction of instantaneous frequencies, *IEEE Trans. Inform. Theory*, **38**: 644–664, (1992)
[21] S. De Luca and E. Fiordilino, Wavelet temporal profile of high order harmonics emitted by a two-level atom in the presence of a laser pulse, *J. Phys. B: At. Mol. Opt. Phys.*, **29**: 3277–3292, (1996)
[22] D.H. Feng, J.R. Klauder and M. Strayer (eds.), *Coherent States: Past, Present and Future (Proc. Oak Ridge 1993)* (World Scientific, Singapore, 1994)
[23] R. Ferrari, Two-dimensional electrons in a strong magnetic field: A basis for single-particle states, *Phys. Rev. B*, **42**: 4598–4609, (1990)
[24] E. Fiordilino and V. Miceli, Temporal evolution of the spectrum emitted by a two-level atom in the presence of a laser field, *J. Mod. Optics*, **43**: 735–751, (1996)
[25] P. Fischer and M. Defranceschi, Iterative process for solving Hartree–Fock equations by means of a wavelet transform, *Appl. Comput. Harm. Anal.*, **1**: 232–241, (1994)
[26] P. Fischer and M. Defranceschi, Representation of the atomic Hartree–Fock equations in a wavelet basis by means of the BCR algorithm, in *Wavelets: Theory, Algorithms, and Applications*, pp. 495–506; ed. C.K. Chui, L. Montefusco and L. Puccio (Academic Press, San Diego, 1994)
[27] S. Goedecker and O.V. Ivanov, Linear scaling solution of the Coulomb problem using wavelets, *Solid State Commun.*, **105**: 665–669, (1998)
[28] X. Gonze, private communication
[29] M. Greiter and I.A. McDonald, Hierarchy of quantized Hall states in double layer electron systems, *Nucl. Phys. B*, **410**: 521–534, (1993)

[30] F.D.M. Haldane, Fractional quantization of the Hall effect: A hierarchy of incompressible quantum fluid states, *Phys. Rev. Lett.*, **51**: 605–608, (1983)
[31] C.R. Handy, D. Bessis and T.D. Morley, Generating quantum energy bounds by the moment method: A linear-programming approach, *Phys. Rev. A*, **37**: 4557–4569, (1988), and related papers
[32] C.R. Handy and R. Murenzi, Continuous wavelet transform analysis of one dimensional quantum bound states from first principles, *Phys. Rev. A*, **54**: 3754–3763, (1996)
[33] C.R. Handy and R. Murenzi, Continuous wavelet transform analysis of quantum systems with rational potentials, *J. Phys. A*, **30**: 4709–4729, (1997)
[34] E. Huens, B. Piraux, A. Bugacov and M. Gajda, Numerical studies of the dynamics of multiphoton processes with arbitrary field polarization: methodological considerations, *Phys. Rev. A*, **55**: 2132–2143, (1997)
[35] K. Kaneda and T. Odagaki, Two-scale relations in one-dimensional crystals and wavelets, *J. Phys. A: Math. Gen.*, **28**: 4389–4406, (1995)
[36] J.R. Klauder and B.S. Skagerstam, *Coherent States – Applications in Physics and Mathematical Physics* (World Scientific, Singapore, 1985)
[37] W. Kohn and L.J. Sham, Self-consistent equations including exchange and correlation effects, *Phys. Rev. A*, **140**: 1133–1138, (1965)
[38] K.C. Kulander, Multiphoton ionization of hydrogen: A time-dependent theory, *Phys. Rev. A*, **35**: 445–447, (1987)
[39] K.C. Kulander, K.J. Schafer and J.L. Krause, Dynamics of short-pulse excitation, ionization and harmonic conversion, in *Super-Intense Laser-Atom Physics*, pp. 95–110; ed. B. Piraux, A. L'Huillier and K. Rzażewski, NATO ASI Series B, **316** (Plenum Press, New York, 1993)
[40] D.G. Lappas, A. Sanpera, J.B. Watson, K. Burnett, P.L. Knight, R. Grobe and J.H. Eberly, Two-electron effects in harmonic generation and ionization from a model He atom, *J. Phys. B: At. Mol. Opt. Phys.*, **29**: L619–L627, (1996)
[41] M. Lewenstein, Ph. Balcou, M.Yu. Ivanov, A. L'Huillier and P.B. Corkum, Theory of high-harmonic generation by low-frequency laser fields, *Phys. Rev. A*, **49**: 2117–2132, (1994)
[42] M. Lewenstein, P. Salières and A. L'Huillier, Phase of the atomic polarization in high-order harmonic generation, *Phys. Rev. A*, **52**: 4747–4754, (1995)
[43] A. L'Huillier and Ph. Balcou, High-order harmonic generation in rare-gases with a 1-ps 1053-nm laser, *Phys. Rev. Lett.*, **70**: 774–777, (1993)
[44] A. L'Huillier, T. Auguste, Ph. Balcou, B. Carré, P. Monot, P. Salières, C. Altucci, M.B. Gaarde, J. Larsson, E. Mevel, T. Starczewski, S. Svanberg, C.-G. Wahlström, R. Zerne, K.S. Budil, T. Ditmire and M.D. Perry, High-order harmonics: a coherent source in the XUV range. *J. Nonlinear Optical Physics and Materials*, **4**: 647–664, (1995)
[45] J. Liandrat, V. Perrier and Ph. Tchamitchian, Numerical resolution of the regularized Burgers equation using the wavelet transform, in *Wavelets and Applications*, pp.420–433; ed. Y. Meyer (Springer, Berlin, and Masson, Paris, 1992)
[46] J.J. Macklin, J.D. Kmetec and C.L. Gordon III, High-order harmonic generation using intense femtosecond pulses, *Phys. Rev. Lett.*, **70**: 766–769, (1993)
[47] R.G. Mani and K. von Klitzing, Fractional quantum Hall effect as an example of fractal geometry in nature, *Z. Phys. B*, **100**: 635–642, (1996)

[48] G. Morandi, *The Role of Topology in Classical and Quantum Physics*, Lecture Notes Phys. **m7** (Springer, Berlin, Heidelberg, 1992)
[49] M. Moshinsky and C. Quesne, Linear canonical transformations and their unitary representations, *J. Math. Phys.*, **12**: 1772–1780, (1971)
[50] M. Rotenberg, Theory and application of Sturmian functions, *Adv. At. Mol. Phys.*, **6**: 233–268, (1970)
[51] R.A. Smith, J.W.G. Tisch, M. Ciarrocca, S. Augst and M.H.R. Hutchinson, Angularly resolved ultra high harmonic generation experiments with picosecond laser pulses, in *Super-Intense Laser-Atom Physics*, pp. 31–41; ed. B. Piraux, A. L'Huillier and K. Rzcażewski, NATO ASI Series B, **316** (Plenum Press, New York, 1993)
[52] T. Starczewski, J. Larsson, C.-G. Wahlström, J.W.G. Tisch, R.A. Smith, J.E. Muffet and M.H.R. Hutchinson, Time-resolved harmonic generation in an ionizing gas, *J. Phys. B: At. Mol. Opt. Phys.*, **27**: 3291–3301, (1994)
[53] W. Sweldens, The lifting scheme: a custom-design construction of biorthogonal wavelets, *Applied Comput. Harm. Anal.*, **3**: 1186–1200, (1996)
[54] R. Taieb, A. Maquet, Ph. Antoine and B. Piraux, Time dependence of harmonic generation by a single atom, in *Super-Intense Laser-Atom Physics IV*; pp. 445–454; ed. H.G. Muller and M.V. Fedorov, NATO ASI Series 3, **13**: (Kluwer, Dordrecht, 1996)
[55] C.J. Tymczak and X.Q. Wang, Orthonormal wavelet bases for quantum molecular dynamics, *Phys. Rev. Lett.*, **78**: 3654–3657, (1997)
[56] B.Ph. van Milligen, C. Hidalgo and E. Sánchez, Nonlinear phenomena and intermittency in plasma turbulence, *Phys. Rev. Lett.*, **74**: 395–398, (1995)
[57] S. Wei and M.Y. Chou, Wavelets in self-consistent electronic structure calculations, *Phys. Rev. Lett.*, **76**: 2650–2653, (1996)
[58] K. Yamaguchi and T. Mukoyama, Wavelet representation for the solution of radial Schrödinger equation, *J. Phys. B: At. Mol. Opt. Phys.*, **29**: 4059–4071, (1996)